The role of CNC surface modification on the structural, thermal and electrical properties of poly(vinylidene fluoride) nanocomposites

M. Rincón-Iglesias[1], *E. Lizundia*[1,2,*], *D. M. Correia*[3,4], *C. M. Costa*[4,5,*], *S. Lanceros-Méndez*[1,6]

[1] BCMaterials, Basque Center Centre for Materials, Applications and Nanostructures, UPV/EHU Science Park, 48940 Leioa, Spain.

[2] Department of Graphic Design and Engineering Projects, Bilbao Faculty of Engineering, University of the Basque Country (UPV/EHU), Bilbao 48013, Spain.

[3] Department of Chemistry and CQ-VR, Universidade de Trás-os-Montes e Alto Douro, 5000-801 Vila Real, Portugal

[4] Centro de Física, Universidade do Minho, 4710-057 Braga, Portugal

[5] Centro de Química, Universidade do Minho, 4710-057 Braga, Portugal

[6] IKERBASQUE, Basque Foundation for Science, 48013 Bilbao, Spain

[*]**Corresponding Authors E-mail:** E. Lizundia (erlantz.liizundia@ehu.eus); C.M. Costa (cmscosta@fisica.uminho.pt)

Abstract

This work reports on the effect of cellulose nanocrystal (CNC) surface charge in the structure and dielectric properties of poly (vinylidene fluoride) (PVDF) nanocomposites. CNCs extracted through sulfuric acid hydrolysis were modified using sodium hydroxide and cationization treatments to yield CNCs with zeta-potential values of -26.1 ± 3.7 and -4.4 ± 0.3 mV in comparison with the original highly-negative -45.2 ±1.1 mV. Nanocomposites with a concentration up to 25 wt% CNC have been obtained through doctor-blade casting followed by room temperature drying. The induced changes on the morphology, structure, thermal and dielectric response depending on the CNC concentration and surface-charge are investigated. CNC incorporation allows obtaining PVDF comprisisng 100 % of γ-phase. Further, an increase of the real dielectric constant ε', dielectric loss *tan* δ and ac conductivity values are observed in the nanocomposites by increasing CNC content. More importantly, these values are further increased upon CNC surface-modification, suggesting the relevance of the interfacial contributions to the dielectric response and that the sulfate half-ester removal to yield –OH groups is able to increase the amount of accumulated charges at the PVDF-CNC interfaces.

Keywords: A: Polymer-matrix composites (PMCs); B: Electrical properties; D: Infrared (IR) spectroscopy; D: X-ray diffraction (XRD); cellulose nanocrystals.

1. Introduction

Poly (vinylidene fluoride) (PVDF) is a semicrystalline thermoplastic with relevant technological electroactive properties for sensor and actuator applications. Its ferroelectric, pyroelectric and piezoelectric properties strongly depend on the type of crystalline polymorph present in the material, which comprises α, β, γ, δ or ε phases [1-3]. Among them, the β-phase is the one with the largest net dipole moment and piezoelectric response [2]. As melt-processing technologies typically result in the formation of the non-polar α-phase, many efforts has been carried out in order to promote the formation of β-phase PVDF [2], including poling [4], thermal treatment [5], stretching [6] or nanocomposite development [7, 8]. The other relevant electroactive phase it the γ phase. This phase shows a piezoelectric response of -7 pC/N and can be obtained by reinforcing PVDF with clays and other fillers [9]. Interestingly, this phase has been gathering increasing attention with applications in the areas of optical sensors and actuators [9, 10].

As particles can be directly incorporated during the fabrication process, nanocomposite development can be seen as one of the preferred approach due to its simplicity. Moreover, the presence of nanofillers typically enhances other technologically relevant macroscopic properties of the hosting matrix such as electrical [11], mechanical [12], thermal [13], optical [14], or barrier properties [15].

The use of inorganic nanofillers (carbon nanotubes, barium titanate or cobalt ferrite, among others) to nucleate the electroactive phases of PVDF has been deeply investigated in the past [16-18]. However, the use of organic nanoparticles remains still in its infancy. In this regard, cellulose nanocrystals (CNCs) could be considered as one of the most promising fillers due to their anisotropic character (large surface-area), renewability, cost-effectivenes, low-density, compostability, mechanical stability with a

high Young´s modulus (130 GPa), and simple surface modification [19-21]. Although CNCs can be extracted from cellulosic sources upon controlled mechanical, chemical or enzymatic disintegration, sulfuric acid hydrolysis is the most commonly used method [22]. This approach yields CNC surfaces with negatively charged half-ester groups (-OSO_3^-). Thanks to the fact that the surface chemistry of CNCs can be easily modified due to the many surface hydroxyl (–OH) groups, tailored functionalities can be incorporated. Additionally, the highly crystalline character of CNCs may help to enhance the inherent the piezoelectric effect of wood, contributing to increase the overall piezoelectric behaviour of the resulting nanocomposite [23].

Till the date several studies have focused on the understanding of how the surface modification of CNCs alters the properties of resulting polymer nanocomposites. For instance, the ionic strength of aqueous CNC dispersions can be modified with surfactants such as cetyltrimethylammonium bromide, allowing their dispersion within solvent/matrices of decreasing polarity [24]. Lizundia et al. reported that the modification of CNC surface charge can lead to enhanced electrochemical performance of CNC/polypyrrole composites [25]. Acetylation was pursued to increase the interfacial adhesion of CNCs with the hosting poly(butylene succinate) matrix [26]. Alanis et al. modified CNCs by means of plasma-surface modification and reported a significantly enhanced impact resistance of the hosting acrylonitrile butadiene styrene polymer matrix [27].

Till the date PVDF /cellulose nanocomposites have been studied for applications as varied as filtration [28], and self-powering electronic textiles [29]. It was found that the addition of microcrystalline cellulose (MCC) induces β-phase PVDF, negatively impacting the mechanical performance [30]. In the case of electrospun PVDF/cellulose nanofibers, the presence of cellulose barely affects the β-phase content and the total

crystallinity of PVDF, although the dielectric constant values markedly increased with cellulose content [31]. Recently, for PVDF/cellulose nanofibril composites it has been demonstrated the nucleation of the PVDF γ-phase, where the thermal and mechanical properties depend on the cellulose nanofibril concentration [32].

Taking into consideration the previous works carried out in the field of PVDF/CNC composites, it results critical to understand how CNCs having different surface charges can serve as heterogeneous nucleation sites for electroactive phases of PVDF. Therefore, CNCs being highly negative, slightly negative and neutral have been incorporated into PVDF at different concentrations and the resulting physico-chemical properties and polymer crystalline conformation of the nanocomposites has been studied. Finally, the dielectric properties have been also investigated.

2. Materials and Methods

2.1. Starting materials

Microcrystalline cellulose with an average particle size of 20 μm (310697-500G), sulphuric acid (95 - 97 %, 30743-1L) and dimethylformamide (DMF) have been supplied by Sigma Aldrich and used as received. Poly (vinylidene fluoride) (PVDF) with a number-average molecular weight of M_w = 570-600 kg•mol^{-1} was purchased from Solvay (Solef 6020).

2.2. CNCs synthesis and CNC surface modification

Cellulose nanocrystals (CNCs) are extracted from microcrystalline cellulose by sulfuric acid hydrolysis followed by sonication [22, 33]. 5 g of commercial microcrystalline cellulose were hydrolyzed in 100 mL of aqueous 64 % (w/w) sulphuric acid solution at 45 °C for 30 min under magnetic stirring at 500 rpm. The reaction was

stopped by adding 1 L of cold distilled water. The suspension was centrifuged at 5000 rpm for 10 min to remove the excess of acid. Colloidal cellulose was obtained via sonication in a Vibracell Sonicator (Sonicsand Materials Inc., Danbury, CT) at 50% output for 10 min. For further purification, the suspension was dialyzed during 7 days using a Visking dialysis membrane with a molecular weight cut off of 12.000-14.000 Da (Medicell Membranes Ltd). An aqueous CNC dispersion with a pH of 2.3 and a concentration of 1.5 % w/w was obtained. As sulfuric acid hydrolysis yields negatively charged CNCs, further modification steps are required to decrease its negative character (see Fig. 1).

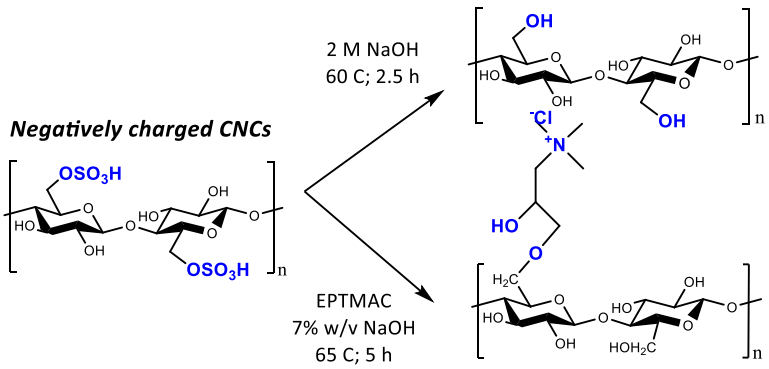

Fig. 1. Water-dispersed CNCs underwent two different surface treatments to obtain surface modified CNCs.

Due to the regioselectivity of the reactions, CNC surface modification is carried out at the C6 position. Slightly negative CNCs were obtained upon the removal of the surface anionic sulfate ester groups ($–OSO_3^-$) by a 2 M NaOH solution at 60 ºC [34]. After 2.5 h the reaction was quenched with 5-fold distilled water and the excess of NaOH was removed by centrifugation as described above. Positive groups onto CNCs were incorporated after the reaction of the C6 carbon atom with epoxypropyltrimethylammonium chloride (EPTMAC) to yield CNCs with cationic hydroxypropyltrimethylammonium chloride substituents [35]. Water dispersed CNCs

where exchanged into a 7% w/v NaOH solution. After 30 minutes at room temperature, 10 mg of EPTMAC were added and it was allowed to react for 5 h at 65 ºC. The reaction was also stopped by adding 5-fold distilled water followed by centrifugation.

In order to incorporate CNCs into PVDF, water-dispersed CNCs have been exchanged to DMF through centrifugation. Firstly, 5 mL of acetone are added to aqueous CNC dispersions before centrifugation at 5000 rpm for 10 min. The supernatants are poured off and the remaining CNCs are washed two times with acetone and three times with DMF using the same centrifuge parameters. Re-suspended solutions are submitted to sonication for 4 min after each step during the solvent exchange to avoid CNC aggregation. DMF-dispersed CNCs where stored at 4 ºC.

2.3. Nanocomposite preparation

PVDF/CNC nanocomposite films were obtained by doctor-blade casting as reported previously [36]. After dissolving the PVDF into DMF, the required amount of CNCs was added to obtain 14 % (by weight) dispersions. After dispersion by magnetic stirring and sonication, the mixtures were deposited by the doctor blade technique onto a clean glass substrate allowing DMF to evaporate at 80 ºC. Neat PVDF films were also prepared for comparison. Samples with an average thickness of 40 ± 10 μm were obtained by this method.

2.4. Characterization

Modified CNCs were observed under a Philips CM120 Biofilter transmission electron microscopy (TEM) with STEM module at an acceleration voltage of 120 kV. A droplet of aqueous CNC suspension (0.1 $mg \cdot mL^{-1}$) was negatively stained with 1% uranyl acetate ($UO_2(CH_3COO)_2$) for 1 min before analysis [33]. CNC surface charge

was determined by Zeta-potential measurements using a Malvern Zetasizer Nano-ZS (0.1 mg·mL^{-1}). PVDF/CNC nanocomposites were observed with a scanning electron microscope (SEM, NanoSEM - FEI Nova 200 (FEG/SEM)) at an accelerating voltage of 15 kV. Before analysis, samples were coated with a gold layer by sputtering with a Polaron SC502 apparatus. Attenuated total reflectance Fourier transform infrared spectroscopy (ATR-FTIR) of PVDF/CNC nanocomposites was carried out in a Jasco FT/IR-4100 system in the range of 4000 - 600 cm^{-1} with a resolution of 2 cm^{-1}. Wide angle X-ray diffraction (WAXD) measurements were performed on a PANalytical Empyrean diffractometer in reflection mode using Cu Kα radiation (λ = 1.5418 Å) and operating at 45 kV and 40 mA. Thermal transitions of nanocomposites were studied with a Netzsch DSC 204 F1 Phoenix differential scanning calorimetry (DSC) under nitrogen flow in the range of 25-200 ºC at a rate of 10 ºC·min^{-1} for both cooling and heating. All samples were measured in 40 µL aluminium pans with perforated lids.

The dielectric response of the materials was obtained by measuring at room temperature the capacity (C) and dielectric losses (*tan δ*) with a Quadtech 1920 LCR precision Meter in the 20 Hz - 1 MHz frequency range with an applied voltage of 0.5 V. 5 mm diameter aluminum electrodes were vacuum evaporated onto both sides of each sample (2% error) to obtain samples with a parallel plate condenser configuration. The real part of the dielectric function (*ε'*) and the real part of the electrical conductivity (*σ'*) were obtained according to:

$$\varepsilon' = \frac{C.d}{\varepsilon_0.A} \quad (1)$$

$$\tan\delta = \frac{\varepsilon''}{\varepsilon'} \quad (2)$$

$$\sigma' = \varepsilon_0 \omega \varepsilon'' \quad (3)$$

where A indicates the plate area, d is a plate distance, ε_0 (8.85×10^{-12} F·m^{-1}) is the permittivity of free space, $\varepsilon' and \varepsilon''$ are the real and imaginary dielectric constant respectively and $\omega=2\pi\nu$ is the angular frequency.

3. Results and discussion

3.1. CNC surface modification

To study the effect of CNC surface charge on the resulting structural and dielectric properties of PVDF/CNC nanocomposites, CNCs having three different surface charges have been obtained upon surface modification as shown in Fig. 1. Fourier transform infrared spectroscopy (FTIR) and wide-angle X-ray diffraction (WAXD) measurements were conducted to confirm the successful modification of CNCs. Fig. 2a shows the FTIR spectra of surface modified CNCs. All three samples present the characteristic peaks of cellulose, with the broad 3650-3200 cm^{-1} band due to the O-H stretching, the 2902 cm^{-1} corresponding to the asymmetric C–H stretching and further bands at 1337 cm^{-1}, 1160 cm^{-1} and 897 cm^{-1} due to C–O–H bending, C–O–C bending and to C–O–C asymmetric stretching respectively [21, 33]. As a result of the NaOH treatment, treated CNCs present a decreased intensity of the 1033 cm^{-1} band, indicating the partial removal of –SO_3 groups from the CNC surfaces [34]. Moreover, two new peaks at 1640 cm^{-1} and 1480 cm^{-1} arise for CNCs modified with EPTMAC. Such bands are indicative of the adsorbed water as a result of cationization-induced hydrophilization and of the C-N vibration of cationic hydroxypropyltrimethylammonium chloride substituents respectively [35].

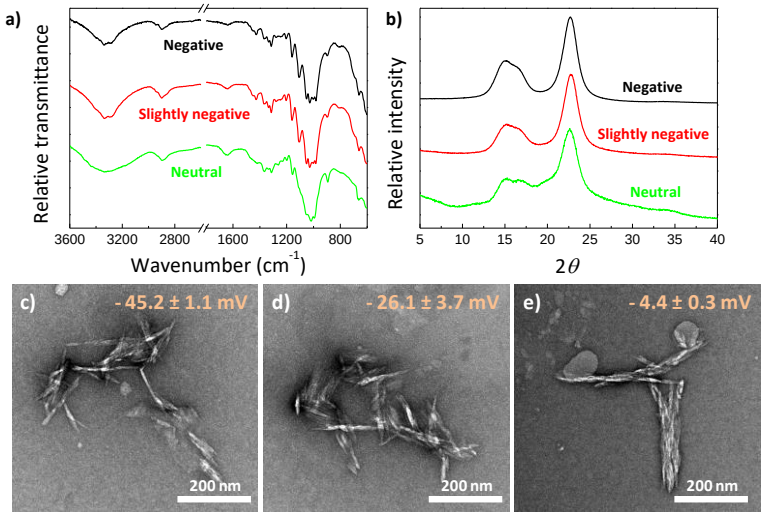

Fig. 2. Characterization of modified CNCs. a) FTIR spectra; b) WAXD patterns and TEM images of c) negative CNCs, d) slightly negative CNCs and e) nearly neutral CNCs. Measured zeta-potential is shown as an inset on the top of TEM images.

Due to the modifications carried out, the initially highly negative CNCs, with a zeta-potential of -45.2 ±1.1 mV leads to slightly negative (-26.1 ± 3.7 mV) and nearly neutral (-4.4 ± 0.3 mV) CNCs after NaOH treatment and NaOH/ EPTMAC treatment. These results suggest that NaOH does not successfully remove all the negatively-charged anionic sulfate ester groups ($–OSO_3^-$) from CNC surfaces as still the overall charge of CNCs remains negative. As a result of that, EPTMAC treatment serves to introduce positively-charged moieties onto CNC surfaces, which may counteract the charge of the remaining negative $–OSO_3^-$ groups to yield neutral CNCs. Despite the surface modification of the CNCs, their crystalline structure and morphological features remain barely unchanged as indicated by the WAXD patterns in Fig. 2b and TEM micrographs in Fig. 2c-e respectively. Indeed, for all three samples WAXD patterns display the characteristic diffraction peaks of cellulose I at 2θ = 14.9º, 16.5º, 22.7º and 34.4º, which correspond to *(1-10), (101), (200)* and *(004)* planes respectively [37, 38]. Additionally, CNCs present a length of 160 ± 35 nm (statistics based on 30 particle

counts) independently of the surface modification, indicating that the initial morphology of CNCs (those extracted upon sulphuric acid hydrolysis) is kept after NaOH and EPTMAC treatment.

3.2. Morphology, physicochemical conformation and crystalline structure of the nanocomposites

The morphological changes of the PVDF/CNC nanocomposites induced by the presence of surface-modified CNCs have been investigated by field-emission scanning electron microscopy (FE-SEM). Accordingly, Fig. 2a-c display the cross-section of cryogenically fractured PVDF/CNC nanocomposites for different negatively charged CNC concentrations (0, 5 and 25 %). For neat PVDF (Fig. 2a), a dense and a relatively smooth surface is observed. Surface roughness increases with CNC concentration as shown in Fig. 2b-c, where an homogeneous distribution of CNCs with no aggregates along the cross-section is observed. Fig. 2d suggests that CNC surface charge does not affect the morphology of PVDF/CNC nanocomposites as no relevant changes are found when comparing with Fig. 2c.

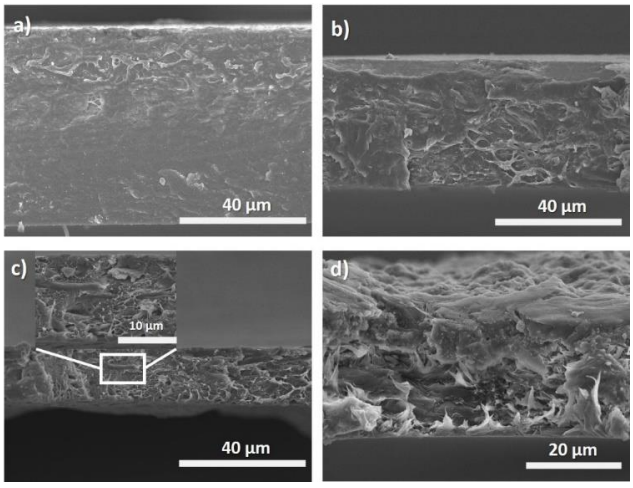

Fig. 2. FE-SEM micrographs of cryogenically fractured PVDF/CNC films with negatively charged CNCs at a concentration of: (a) 0%; (b) 5 % and (c) 25 %. (d) PVDF/CNC with neutral CNCs at 25 %.

To study the influence of the CNC charge on the resulting PVDF crystalline form a Fourier transform infrared spectroscopy (FTIR) analysis was performed. The infrared spectra of the PVDF/CNC nanocomposites are shown in Fig. 3. The CNC absorption bands at 3650-3200 cm^{-1} are assigned to the O-H stretching vibration of CNC, indicating the presence of the CNC into the matrix [39]. As expected, an increase in the CNC characteristic absorption bands occurs when the CNC amount increases. Independently of the CNC charge, the main characteristic PVDF absorption bands are observed for the different PVDF/CNC nanocomposites with different CNC charges. The absorption band at ~1403 cm^{-1} is attributed to the wagging vibration of the CH_2 group. The absorption bands at 796 and 760 cm^{-1} are ascribed to the PVDF α phase. The absorption bands at 1245, 833 and 811 cm^{-1} are assigned to the γ phase characterized by a $T_3GT_3G`$ conformation, being an indicative that neat and PVDF/CNC nanocomposites crystallize into the γ phase, independently of the CNC charge [40] (observed in detail latter in the Fig. 3b). From all the FTIR spectra it is also observed the absence of an absorption band at 1275 cm^{-1} [40], characteristic of the β phase (for PVDF having low molecular weight β-phase fraction decreases with increasing evaporation temperature due to different evaporation rates [41, 42]). For evaporation temperatures above 90 ºC, the evaporation rate is high and there is no enough time for nucleation of the more stable α-phase phase, and the polymers growths into a metastable phase [42]. These results indicate that the solvent evaporation at 90 ºC favors PVDF crystallization process into the γ phase crystalline structure due to significant polymer chain entanglements. It is also to notice, that independently of the CNC charge (Fig. 3c and 3d), a decrease on the α phase absorption bands intensity is observed, indicating that the γ phase becomes the predominantly phase in the PVDF/CNC blends with increasing CNC content.

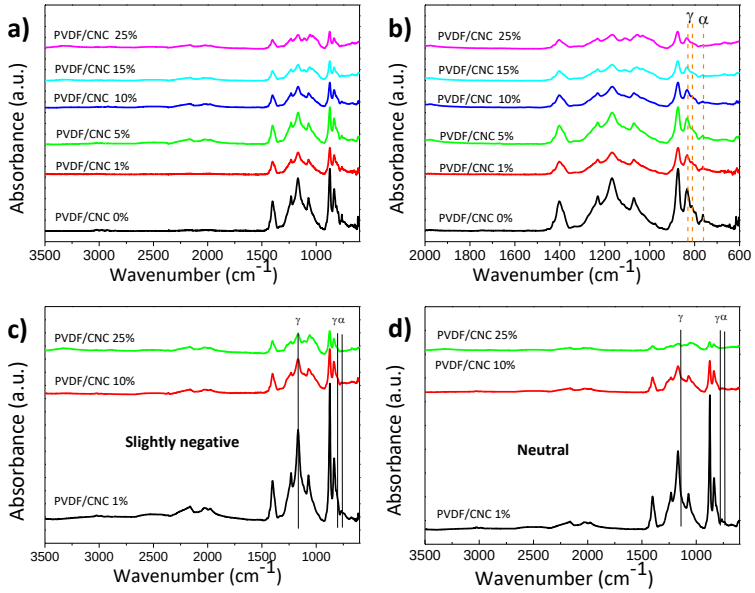

Fig. 3. FTIR spectra of PVDF/CNC nanocomposites for different CNC surface charges: a) PVDF/CNC having negatively charged CNCs; b) enlarged FTIR spectra of PVDF/CNC with negatively charged CNCs; c) PVDF/CNC comprising slightly negative CNCs and d) PVDF/CNC comprising neutral CNCs.

The influence of CNC addition on the amount of γ phase was quantified from FTIR results according the following Equation:

$$F(\gamma) = \frac{A_\gamma}{\left(K_\gamma / K_\alpha\right) A_\alpha + A_\gamma} \quad (4)$$

where A_α and A_γ represent the absorbencies at 766 and 833 cm^{-1} corresponding to α- and γ-phases and Kγ and Kα are the absorption coefficients being 0.365 and 0.150 μm^{-1}, respectively [1]. As expected, neat PVDF crystallizes mainly in the γ phase, reaching a γ phase content of 86%. Similar results are observed for the PVDF/CNC blends with different CNC charges, being observed a PVDF crystallization into the γ phase. For the nanocomposite bearing negatively charged CNCs, the γ phase content increases up to 90% with the CNC amount increase until 5%. For CNC concentrations larger than 5%, the PVDF tends to crystallize only in the γ phase as shown Table 1. Similarly, the slightly negative (-26.1 ± 3.7 mV) and neutral (-4.4 ± 0.3 mV) CNCs induce a PVDF

crystallization in the γ phase. These results suggest that the negative charge of the CNC interacts with the PVDF CH_2 groups and the positively CNC charges with the negative CF_2 groups. However, these interactions are weak as similar results are observed for the samples containing the neutral CNC.

The effect of CNC charge and concentration on the resulting PVDF crystallization has been evaluated through X-ray diffraction (XRD). Fig. 4 shows the obtained XRD patterns for the PVDF and PVDF/CNC nanocomposites comprising different charges. From Fig. 4a it is observed that PVDF displays two diffraction peaks at 2θ = 18.9º and 39.4º and a stronger peak at 2θ =20.5º. These diffraction peaks are ascribed to the PVDF *(020)*, *(211)* and *(110/101)*, respectively, and are associated with the monoclinic γ phase respectively. These results are in agreement with the FTIR results where it was observed that PVDF mainly crystallizes in this phase. Similar results are observed for the PVDF/CNC negatively charged containing 5% of CNC. For higher CNC ratios (10-25%) the diffraction peaks at 14.9º, 16.5º and 22.7º are attributed to the *(1-10)*, *(101)* and *(200)* crystallographic planes of CNC respectively (cellulose I form), increasing the peaks intensity with the CNC amount increase [28]. Similar results are observed for the PVDF/neutral (Fig. 4b) and positive (Fig. 4c) CNC nanocomposites, where the intensity of the diffraction peaks arising from CNC increase with CNC fraction.

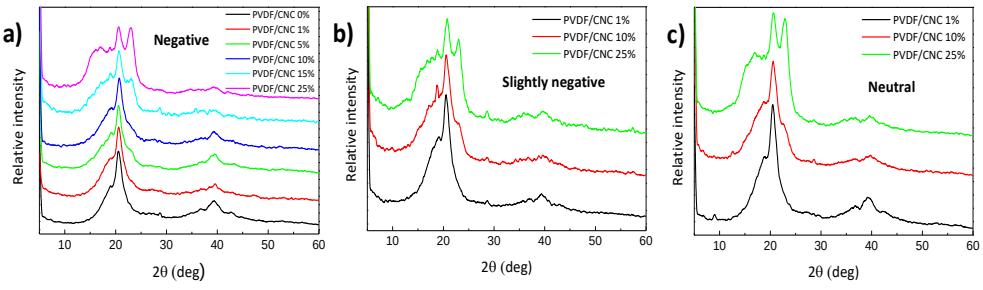

Fig. 4. XRD patterns of PVDF/CNC nanocomposites for different CNC surface charges: a) negatively charged CNCs; b) slightly negative CNCs and c) neutral CNCs.

311 *3.3. Thermal properties*

312 The effect of CNC surface charge on the degree of crystallinity and melting
313 temperature of the PVDF/CNC nanocomposites was determined by differential
314 scanning calorimetry (DSC). Fig. 5a shows the DSC heating thermograms of
315 PVDF/CNC nanocomposites where the endothermic curves represent the melting
316 process of PVDF phase achieved at 170-180ºC. A single peak is observed for all
317 PVDF/CNC nanocomposites except for the nanocomposite with 1% where the existence
318 of the double peak in the PVDF melting behavior can be attributed to the increase of
319 lamellae thickness, i.e. the interlamella diffusion of the polymer chains [43, 44].

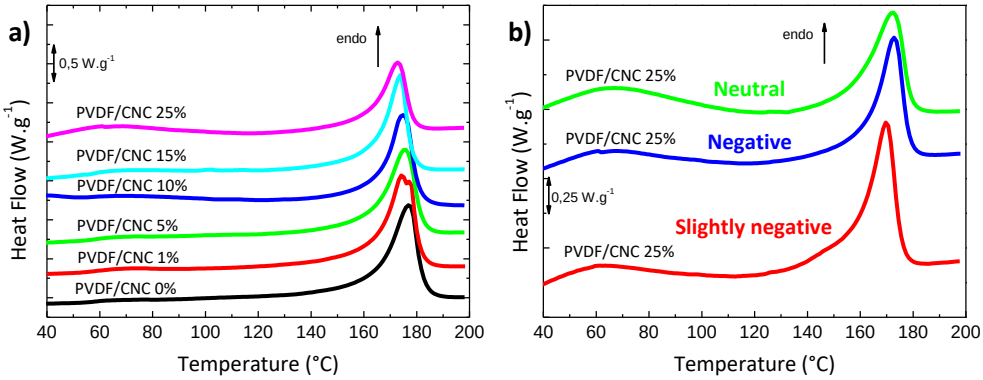

320

321 **Fig. 5.** DSC thermograms for PVDF/CNC nanocomposites for different compositions and CNC surface
322 charges: a) negatively charged CNCs and b) a comparison between PVDF/CNC 25% nanocomposites
323 containing strongly negative, slightly negative and neutral CNCs.

324

325 It is observed that the melting temperature of the PVDF polymer is not affected by
326 the addition of CNC filler and its value remains between 173-177 ºC within the
327 experimental error. This behaviour is also observed for other all the nanocomposites
328 bearing CNCs with different surface charges as shown in Fig. 5b for 25 wt% of CNC.
329 Indeed, no changes on the thermal transitions are observed upon CNC surface
330 modification. To get further insights on the effect of CNC surface charge on the

structure of PVDF, the degree of crystallinity for all PVDF/CNC nanocomposites was determined through the following equation:

$$X_c(\%) = \frac{\Delta H_f}{\Delta H_f^0 \cdot W_m} \quad (5)$$

where ΔH_f is the fusion enthalpy measured during the heating scan, W_m is the PVDF matrix weight fraction and ΔH_f^0 is the heat of fusion of an infinitely thick PVDF crystal (set at 104.6 $J \cdot g^{-1}$) [1]. Accordingly, Table 1 shows the degree of crystallinity for all PVDF/CNC nanocomposites. It is observed that the degree of crystallinity remains independent of the CNC amount and surface charge, which can be explained by the fact that CNC filler does not act as nucleating agent and does not affect the melting behaviour of PVDF matrix.

Table 1. Degree of crystallinity (X_c) and γ-phase content for all PVDF/CNC nanocomposites.

Sample	X_c ± 3 (%)	γ-phase ± 2 (%)
PVDF	48	86
PVDF/CNC (negative) 1%	44	90
PVDF/CNC (negative) 5%	43	100
PVDF/CNC (negative) 10%	40	100
PVDF/CNC (negative) 15%	41	100
PVDF/CNC (negative) 25%	44	100
PVDF/CNC (slightly negative) 25%	46	100
PVDF/CNC (neutral) 25%	44	100

3.4. Dielectric properties

The dielectric behaviour of PVDF/CNC nanocomposites in the frequency range of 20 Hz to 1 MHz at 25ºC was evaluated to study the effect of CNCs on the electrical properties of the films. Fig. 6a shows the variation of the ε' for all PVDF/CNC nanocomposites with negative charge as a function of frequency. Independently of the

CNC amount, the dielectric constant decreases with increasing frequency as a result of the electrical relaxation of the dipoles as frequency increases. It is verified that the dielectric constant depends of the CNC amount as it increases with increasing CNC content due to the increased space charge (Maxwell-Wagner-Siller (MWS) polarization) and polarization contributions by the hydroxyl groups (-OH) present in the cellulose [45]. In addition, at low frequency, the high dielectric constant value for 25% CNC content is ascribed to the large interfacial charge polarization between the PVDF matrix and the CNC fillers.

For 1% of CNC, Fig. 6b shows that CNC surface treatment barely affects the dielectric behavior of PVDF/CNC nanocomposites. For 10% of CNC, on the contrary, it is observed that surface treatment affects the dielectric behavior as the removal of ester groups increases the dielectric constant as a result of the presence of more polar -OH groups that increase dipole-dipole interactions and interfacial polarization between PVDF polymer and CNCs [46].

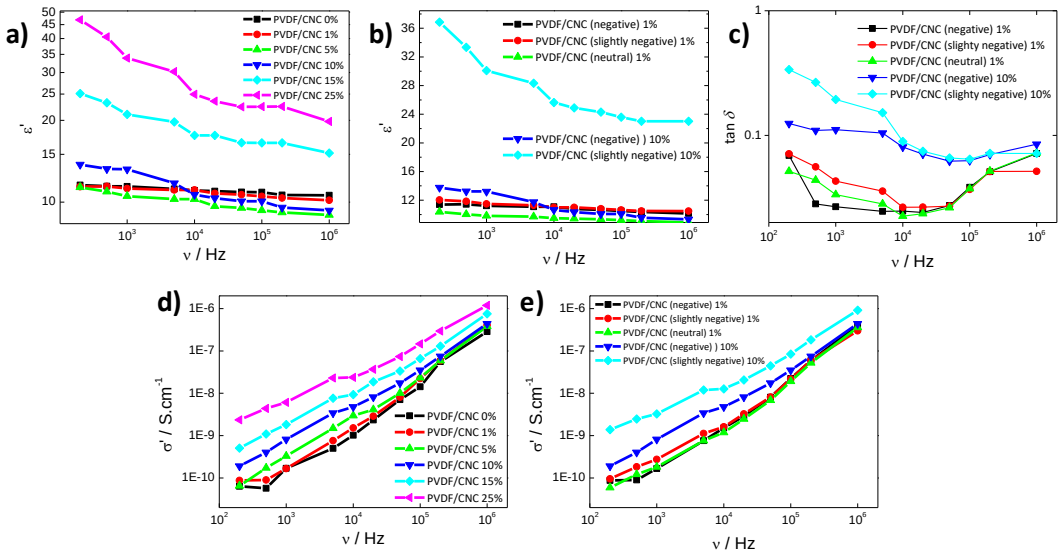

Fig. 6. (a) Real dielectric constant, (c) dielectric loss and (d) conductivity values as a function of frequency for PVDF/CNC nanocomposites having negatively charged CNCs. (b) Real dielectric constant, (c) dielectric loss and (e) conductivity values as a function of frequency for PVDF/CNC nanocomposites having surface modified CNCs.

The dielectric loss (*tan δ*) as a function of frequency for PVDF/CNC nanocomposites is shown in Fig. 6c. It is noticed that the dielectric tangent loss increases with increasing CNC amount due to the increased the space charge polarization associated with interfacial polarization between filler particles and PVDF polymer. For modified CNCs, the dielectric tangent loss also increases with CNC amount. It is worthy to note that for the 10% nanocomposite *tan δ* results much larger (up to an order of magnitude larger) upon CNC surface modification. This can be explained by the fact that surface treatment increases the amount of accumulated charges at the PVDF-CNC interface thanks to higher amount of the polar groups originated by treatment (sulfate half-ester removal to yield –OH groups) [47].

Regarding the electrical AC conductivity values represented in Fig. 6d and 6e, increased electrical AC conductivity is observed with increasing the CNC concentration and CNC surface treatment. The AC electrical conductivity increases with frequency in nearly four orders of magnitude in the measured frequency range, showing a strong contribution of confined dynamics to the electrical conductivity, compatible with Maxwell-Wagner-Siller (MWS) polarization contributions [48-50]. For PVDF/CNC nanocomposites, the conduction mechanism occurs through the hopping of the charge carrier in localized states that increase for higher CNC concentration (Fig. 6d) and for surface treatment that increases the polar -OH groups (Fig. 6e).

The AC conductivity behaviour can be described by Jonscher power-law [51]:

$$\sigma'(\omega) \propto \omega^n, n \leq 1 \quad (6)$$

where ω is the angular frequency and n ranges between $0 < n < 1$, characterizing the hopping conduction mechanism [52]. For PVDF/CNC nanocomposites with negatively charged CNCs, the n value increases with CNC concentration and ranges from 0.5 to 0.9 due to the increase of charge carriers in localized states. For 10 wt% of CNC with

different surface treatment, the *n* value is 0.74 to 0.80, the addition of polar groups affecting the mobility of the charge carriers.

Conclusions

The development of PVDF-based nanocomposites comprising surface-modified CNCs is here presented. Based on NaOH and cationization treatments, the initial highly negative CNCs arising from the sulfuric acid-induced hydrolysis leads to slightly negative and nearly neutral (zeta potential values of -45.2 ±1.1 mV, -26.1 ± 3.7 mV and -4.4 ± 0.3 mV) CNCs. Based on FTIR, XRD and DSC results, no structural changes are achieved upon the incorporation of CNCs into PVDF through doctor blade casting approach. All samples showed the presence of the electroactive γ phase with a X_c crystalline fraction in PVDF ranging from 40 to 48 %. Dielectric spectroscopy analyses show a continuous increase on the real dielectric constant, dielectric loss and ac conductivity values after CNC incorporation due to the increase of the charge carrier concentration and ionic conductivity arising from CNCs. Interestingly, the real dielectric constant, dielectric loss and ac conductivity values can be further increased upon CNC surface modification. Such results are explained in terms of $–OSO_3H$ group removal from CNCs, which enable the presence of additional polar –OH groups which can interact with PVDF matrix. This work provides novel cues for the development of cellulose-based multifunctional materials with enhanced electroactive response.

Data availability

All the data used to support the findings of this study are included within the article.

Acknowledgements

The authors thank the FCT (Fundação para a Ciência e Tecnologia) for financial support under the framework of Strategic Funding grants UID/FIS/04650/2019, UID/EEA/04436/2013 and UID/QUI/0686/ 2016; and projects no. PTDC/BTM-MAT/28237/2017; PTDC/EMD-EMD/28159/2017 and PTDC/FIS-MAC/28157/2017. The authors also thank the FCT for financial Support under grants SFRH/BPD/121526/2016 (D.M.C.) and SFRH/BPD/112547/2015 (C.M.C.) as well POCH and European Union. Financial support from the Spanish Ministry of Economy and Competitiveness (MINECO) through project MAT2016- 76039-C4-3-R (AEI/FEDER, UE) (including FEDER financial support) and from the Basque Government Industry and Education Departments under the ELKARTEK, HAZITEK and PIBA (PIBA-2018-06) programs, respectively, is also acknowledged

References

[1] P. Martins, A.C. Lopes, S. Lanceros-Mendez, Electroactive phases of poly(vinylidene fluoride): Determination, processing and applications, Progr. Polym. Sci. 39(4) (2014) 683-706.
[2] C. Ribeiro, C.M. Costa, D.M. Correia, J. Nunes-Pereira, J. Oliveira, P. Martins, R. Gonçalves, V.F. Cardoso, S. Lanceros-Méndez, Electroactive poly(vinylidene fluoride)-based structures for advanced applications, Nat. Protoc. 13(4) (2018) 681-704.
[3] Z. Cui, N.T. Hassankiadeh, Y. Zhuang, E. Drioli, Y.M. Lee, Crystalline polymorphism in poly(vinylidenefluoride) membranes, Progr. Polym. Sci. 51 (2015) 94-126.
[4] Y. Jiang, Y. Ye, J. Yu, Z. Wu, W. Li, J. Xu, G. Xie, Study of thermally poled and corona charged poly(vinylidene fluoride) films, Polym. Eng. Sci. 47(9) (2007) 1344-1350.
[5] S. Satapathy, S. Pawar, P.K. Gupta, K.B. Rvarma, Effect of annealing on phase transition in poly(vinylidene fluoride) films prepared using polar solvent, B. Mater. Sci. 34(4) (2011) 727-733.
[6] V. Sencadas, R. Gregorio, S. Lanceros-Méndez, α to β phase transformation and microestructural changes of PVDF films induced by uniaxial stretch, J. Macromol. Sci. B 48(3) (2009) 514-525.
[7] C.-W. Tang, B. Li, L. Sun, B. Lively, W.-H. Zhong, The effects of nanofillers, stretching and recrystallization on microstructure, phase transformation and dielectric properties in PVDF nanocomposites, Eur. Polym. J. 48(6) (2012) 1062-1072.
[8] D.R. Dillon, K.K. Tenneti, C.Y. Li, F.K. Ko, I. Sics, B.S. Hsiao, On the structure and morphology of polyvinylidene fluoride–nanoclay nanocomposites, Polymer 47(5) (2006) 1678-1688.
[9] A.C. Lopes, C.M. Costa, C.J. Tavares, I.C. Neves, S. Lanceros-Mendez, Nucleation of the Electroactive γ Phase and Enhancement of the Optical Transparency in Low Filler Content Poly(vinylidene)/Clay Nanocomposites, J. Phys. Chem. C 115(37) (2011) 18076-18082.
[10] Z. Tan, C. Fu, Y. Gao, J. Qian, W. Li, X. Wu, H. Chu, C. Chen, W. Nie, X. Ran, Modifications of Gamma poly (vinylidene fluoride) (γ-PVDF) films by high-energy electron beam irradiation, Radiat. Phys. Chem. 153 (2018) 258-268.

[11] E. Lizundia, R. Sarasua, F. D 'angelo, A. Orlacchio, S. Martino, M. Kenny Josè, I. Armentano, Biocompatible Poly(L-lactide)/MWCNT Nanocomposites: Morphological Characterization, Electrical Properties, and Stem Cell Interaction, Macromol. Biosci. 12(7) (2012) 870-881.
[12] R. Sengupta, M. Bhattacharya, S. Bandyopadhyay, A.K. Bhowmick, A review on the mechanical and electrical properties of graphite and modified graphite reinforced polymer composites, Prog. Polym. Sci. 36(5) (2011) 638-670.
[13] X. Cai, Z. Jiang, X. Zhang, T. Gao, K. Yue, X. Zhang, Thermal property improvement of polytetrafluoroethylene nanocomposites with graphene nanoplatelets, RSC Adv. 8(21) (2018) 11367-11374.
[14] E. Lizundia, A. Urruchi, J.L. Vilas, L.M. Leon, Increased functional properties and thermal stability of flexible cellulose nanocrystal/ZnO films, Carbohydr. Polym. 136 (2016) 250-258.
[15] E. Lizundia, J.L. Vilas, A. Sangroniz, A. Etxeberria, Light and gas barrier properties of PLLA/metallic nanoparticles composite films, Eur. Polym. J. 91 (2017) 10-20.
[16] N. Jia, Q. Xing, G. Xia, J. Sun, R. Song, W. Huang, Enhanced β-crystalline phase in poly(vinylidene fluoride) films by polydopamine-coated $BaTiO_3$ nanoparticles, Mat. Let. 139 (2015) 212-215.
[17] P. Martins, C.M. Costa, M. Benelmekki, G. Botelho, S. Lanceros-Mendez, On the origin of the electroactive poly(vinylidene fluoride) β-phase nucleation by ferrite nanoparticles via surface electrostatic interactions, CrystEngComm 14(8) (2012) 2807-2811.
[18] Z. Zhao, W. Zheng, W. Yu, B. Long, Electrical conductivity of poly(vinylidene fluoride)/carbon nanotube composites with a spherical substructure, Carbon 47(8) (2009) 2118-2120.
[19] E. Lizundia, E. Meaurio, J.L. Vilas, Grafting of Cellulose Nanocrystals, Multifunctional Polymeric Nanocomposites Based on Cellulosic Reinforcements (2016), 61-113.
[20] A. Dufresne, Nanocellulose: A new ageless bionanomaterial, Mater. Today 16(6) (2013) 220-227.
[21] E. Lizundia, U. Goikuria, J.L. Vilas, F. Cristofaro, G. Bruni, E. Fortunati, I. Armentano, L. Visai, L. Torre, Metal Nanoparticles Embedded in Cellulose Nanocrystal Based Films: Material Properties and Post-use Analysis, Biomacromol. 19(7) (2018) 2618-2628.
[22] Y. Habibi, L.A. Lucia, O.J. Rojas, Cellulose nanocrystals: Chemistry, self-assembly, and applications, Chem. Rev. 110(6) (2010) 3479-3500.
[23] F. Kollmann, V. A. Bazhenov: Piezoelectric Properties of Wood (Authorized Translation from the Russian). Consultants Bureau, New York 1961. 180 S., 4°, 55 Abb. Preis: $ 9.50, Zeitschrift für Elektrochemie, Berichte der Bunsengesellschaft für physikalische Chemie 66(6) 522-523.
[24] Surface modification of cellulose nanocrystals with cetyltrimethylammonium bromide, Nord. Pulp Pap. Res. J.29 (2014) 46.
[25] E. Lizundia, T. D. Nguyen, Jose L. Vilas, W.Y. Hamad, M.J. MacLachlan, Chiroptical, morphological and conducting properties of chiral nematic mesoporous cellulose/polypyrrole composite films, J. Mat. Chem. A 5(36) (2017) 19184-19194.
[26] S.Y. Cho, M.E. Lee, H.W. Kwak, H.-J. Jin, Surface-Modified Cellulose Nanocrystal-incorporated Poly(butylene succinate) Nanocomposites, Fibers and Polymers 19(7) (2018) 1395-1402.
[27] A. Alanis, J.H. Valdés, N.-V. María Guadalupe, R. Lopez, R. Mendoza, A.P. Mathew, R. Díaz de León, L. Valencia, Plasma surface-modification of cellulose nanocrystals: a green alternative towards mechanical reinforcement of ABS, RSC Adv. 9(30) (2019) 17417-17424.
[28] H. Bai, X. Wang, Y. Zhou, L. Zhang, Preparation and characterization of poly(vinylidene fluoride) composite membranes blended with nano-crystalline cellulose, Pro. Nat. Sci. Mater. 22(3) (2012) 250-257.
[29] D. Ponnamma, H. Parangusan, A. Tanvir, M.A.A. AlMa'adeed, Smart and robust electrospun fabrics of piezoelectric polymer nanocomposite for self-powering electronic textiles, Mater. Des. 184 (2019) 108176.
[30] X.G. Tang, M. Hou, J. Zou, R. Truss, Poly(vinylidene Fluoride)/Microcrystalline Cellulose Nanocomposites with Enhanced Compatibility and Properties, Key Eng. Mater. 471-472 (2011) 355-360.
[31] A.A. Issa, M. Al-Maadeed, A.S. Luyt, M. Mrlik, M.K. Hassan, Investigation of the physico-mechanical properties of electrospun PVDF/cellulose (nano)fibers, J. Appl. Polym. Sci. 133(26) (2016) 43594.

[32] E. Barnes, J.A. Jefcoat, E.M. Alberts, M.A. McKechnie, H.R. Peel, J.P. Buchanan, C.A. Weiss Jr., K.L. Klaus, L.C. Mimun, C.M. Warner, Effect of Cellulose Nanofibrils and TEMPO-mediated Oxidized Cellulose Nanofibrils on the Physical and Mechanical Properties of Poly(vinylidene fluoride)/Cellulose Nanofibril Composites, Polymers 11(7) (2019) 1091.
[33] E. Lizundia, J.L. Vilas, L.M. Leon, Crystallization, structural relaxation and thermal degradation in Poly(L-lactide)/cellulose nanocrystal renewable nanocomposites, Carbohydr. Polym. 123 (2015) 256-265.
[34] N. Lin, A. Dufresne, Surface chemistry, morphological analysis and properties of cellulose nanocrystals with gradiented sulfation degrees, Nanoscale 6 (2014) 5384-5393.
[35] M. Hasani, E.D. Cranston, G. Westman, D.G. Gray, Cationic surface functionalization of cellulose nanocrystals, Soft Matter 4(11) (2008) 2238.
[36] M. Rincon-Iglesias, E. Lizundia, S. Lanceros-Mendez, Water-Soluble Cellulose Derivatives as Suitable Matrices for Multifunctional Materials, Biomacromol. 20(7) (2019) 2786-2795.
[37] M.A. Lucchini, E. Lizundia, S. Moser, M. Niederberger, G. Nystrom, Titania-Cellulose Hybrid Monolith for In-Flow Purification of Water under Solar Illumination, ACS Appl. Mater. Interfaces 10(35) (2018) 29599-29607.
[38] W.Y. Hamad, T.Q. Hu, Structure-process-yield interrelations in nanocrystalline cellulose extraction, Can. J. Chem. Eng. 88(3) (2010) 392-402.
[39] R. Gonçalves, E. Lizundia, M.M. Silva, C.M. Costa, S. Lanceros-Méndez, Mesoporous Cellulose Nanocrystal Membranes as Battery Separators for Environmentally Safer Lithium-Ion Batteries, ACS Appl. Energy Mat. 2(5) (2019) 3749-3761.
[40] X. Cai, T. Lei, D. Sun, L. Lin, A critical analysis of the α, β and γ phases in poly(vinylidene fluoride) using FTIR, RSC Adv. 7(25) (2017) 15382-15389.
[41] J.C.C. Ferreira, T.S. Monteiro, A.C. Lopes, C.M. Costa, M.M. Silva, A.V. Machado, S. Lanceros-Mendez, Variation of the physicochemical and morphological characteristics of solvent casted poly(vinylidene fluoride) along its binary phase diagram with dimethylformamide, J. Non-Cryst. Solids 412 (2015) 16-23.
[42] R. Gregorio, E.M. Ueno, Effect of crystalline phase, orientation and temperature on the dielectric properties of poly (vinylidene fluoride) (PVDF), J. Mater. Sci. 34(18) (1999) 4489-4500.
[43] C. Marega, A. Marigo, Influence of annealing and chain defects on the melting behaviour of poly(vinylidene fluoride), Eur. Polym. J. 39(8) (2003) 1713-1720.
[44] M. Hikosaka, S. Rastogi, A. Keller, H. Kawabata, Investigations on the crystallization of polyethylene under high pressure: Role of mobile phases, lamellar thickening growth, phase transformations, and morphology, J. Macromol. Sci. B 31(1) (1992) 87-131.
[45] A.M. Abdel-karim, A.H. Salama, M.L. Hassan, Electrical conductivity and dielectric properties of nanofibrillated cellulose thin films from bagasse, J. Phys. Org. Chem. 31(9) (2018) e3851.
[46] G.-Y. Yun, J.-H. Kim, J. Kim, Dielectric and polarization behaviour of cellulose electro-active paper (EAPap), J. Phys. D 42(8) (2009) 082003.
[47] E.M. Godzhaev, A.M. Magerramov, S.S. Osmanova, M.A. Nuriev, E.A. Allakhyarov, Charge state of composites based on polyethylene with semiconductor filler TlInSe2, Surf. Eng. Appl. Elect. 43(2) (2007) 148-151.
[48] S.F. Mendes, C.M. Costa, R.S. i Serra, A.A. Baldalo, V. Sencadas, J.L. Gomez-Ribelles, R. Gregorio, S. Lanceros-Méndez, Influence of filler size and concentration on the low and high temperature dielectric response of poly(vinylidene fluoride) /$Pb(Zr_{0.53}Ti_{0.47})O_3$ composites, J. Polym. Res. 19(9) (2012) 9967.
[49] A.C. Lopes, C.M. Costa, R.S.i. Serra, I.C. Neves, J.L.G. Ribelles, S. Lanceros-Méndez, Dielectric relaxation, ac conductivity and electric modulus in poly(vinylidene fluoride)/NaY zeolite composites, Solid State Ion. 235 (2013) 42-50.
[50] V. Sencadas, S. Lanceros-Méndez, R. Sabater i Serra, A. Andrio Balado, J.L. Gómez Ribelles, Relaxation dynamics of poly(vinylidene fluoride) studied by dynamical mechanical measurements and dielectric spectroscopy, Eur. Phys. J. E 35(5) (2012) 41.
[51] A.K. Jonscher, The 'universal' dielectric response, Nature 267(5613) (1977) 673-679.
[52] R.H. Chen, L.-F. Chen, C.-T. Chia, Impedance spectroscopic studies on congruent $LiNbO_3$ single crystal, J. Phys. Condens. Matter 19(8) (2007) 086225.